Characterization of soil stiffness anisotropy at small strains based on phase velocities of shear waves measured by novel testing apparatus

Junming Liu[1#], *Masahide* Otsubo[2], and *Reiko* Kuwano[3]

[1] *Department of Civil Engineering, The University of Tokyo, 7-3-1 Hongo, Bunkyo-ku, Tokyo 113-8654, Japan*
[2] *Public Works Research Institute, 1-6 Minamihara, Tsukub, Ibaraki-ken, 305-8516, Japan*
[3] *Institute of Industrial Science, The University of Tokyo, 4-6-1 Komaba, Meguro-ku, Tokyo 153-8505, Japan*
[#] *Corresponding author: j-liu@iis.u-tokyo.ac.jp*

ABSTRACT

For the characterization of soil stiffness anisotropy at small strains and the calculation of soil elastic constants derived from the cross-anisotropic model, it is important to obtain stress wave phase velocities of soils in both principal and oblique directions. This study developed an original eight-prismatic shape apparatus equipped with disk-shaped shear plates to measure shear (S-) wave phase velocities (V_{phase}) in multiple directions, and four granular materials of various shapes were tested by this apparatus under isotropic confinement. Experimental results confirm the capability of the new apparatus and reveal that both S-wave propagation and oscillation directions are sensitive to soil inner fabric, i.e., V_s changes with the variation of either S-wave propagation or oscillation direction. Based on the experimental observations, it is suggested to keep the same S-wave oscillation direction when measuring V_s in multiple propagation directions so that the corresponding shape of the S-wave surface (polar plots of V_s in arbitrary propagation directions) is more precise to reflect the small-strain stiffness anisotropy of soils.

Keywords: granular soil; small-strain stiffness anisotropy; phase velocity; soil testing apparatus.

1. Introduction

Most soils exhibit cross-anisotropic elasticity with a vertical axis of symmetry under very small-strain conditions (<0.001% strain) due to either the sedimentation of particles or anisotropic stress states. Understanding the small-strain anisotropy of soils is significant because it has nonnegligible influences on ground deformation patterns and seismic responses (Nishimura et al., 2017; Nemat-Nasser and Takahashi, 1984).

In both soil element testing and field investigation, shear (S-) wave propagation has been widely adopted to obtain the small-strain stiffness of soils and evaluate soils' anisotropic behavior according to the relationship that

$$G_{ij}=\rho V_{s,ij}^2 \quad (1)$$

where G_{ij} is the shear modulus calculated by S-wave velocity $V_{s,ij}$ with propagation and oscillation in i and j directions, respectively, and ρ is the soil density.

In addition to S-waves propagating in horizontal and vertical directions, researchers attempt to measure V_s at an oblique angle to the principal stress directions, by which the independent elastic constants of the soil cross-anisotropic model can be obtained (Bellotti et al., 1996; Sadek et al., 2007), and the small-strain anisotropy of soils can be visualized and predicted by plotting V_s surface (Fioravante, 2000; Chamorro-Zurita et al., 2020). However, in previous studies, the ray velocity V_{ray} calculated directly from wave travel time and distance between bender elements which were not faced in line was used to approximately represent the phase velocity V_{phase} that is required for obtaining the elastic constants as shown in Fig. 1. The relationship between these two velocities is expressed by the following equation

$$V_{phase}=\cos\theta V_{ray} \quad (2)$$

On the other hand, bender elements will generate P-wave components which will contaminate S-wave signals and disturb the evaluation of V_{phase} (Lee and Santamarina, 2005).

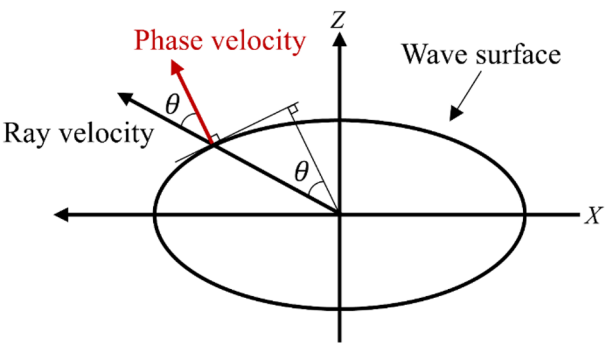

Figure 1. Sketch of ray velocity and phase velocity on the wave surface from a point source in an anisotropic medium.

Based on the necessity for precise evaluation of soil small-strain stiffness anisotropy, this study develops a novel eight-prismatic shape apparatus equipped with

multiaxial piezoelectric shear plates to measure the S-wave phase velocities in both principal (*X*, *Y*, *Z*) and oblique directions. Four kinds of granular materials with different shapes are tested to examine the capability of the apparatus and explore the correlation between soil inner fabric and S-wave propagation directions.

2. Tested materials

Four kinds of granular materials with obvious shape differences, spherical glass beads, Toyoura sand, basmati rice, and wild rice, were tested in this contribution. Images of each material are provided in Fig. 2. The aspect ratio (*AR* = length of minor axis / major axis) is used to quantitatively describe the material shapes as listed in Table 1 with other physical properties. Besides the shape difference, the tested materials also have various particle sizes. Nevertheless, this study assumes that V_s will not be influenced by particle size based on the observations of Yang and Gu (2013) and Dutta et al. (2019).

Table 1. Physical properties of tested materials

Material	D_{50} (mm)	G_s	e_{max}	e_{min}	*AR*
Glass beads	0.20	2.50	0.71	0.54	0.93
Toyoura sand	0.24	2.64	0.94	0.57	0.59
Basmati rice	7.10 (major axis)	1.47	0.81	0.54	0.22
wild rice	11.27 (major axis)	1.47	0.95	0.61	0.16

Although basmati rice and wild rice are not geotechnical materials, they were adopted in this study to explore some relatively large degree of fabric anisotropy that is hard to be observed in natural soils. Referring to the micro-CT images of basmati rice and wild rice in Fig.2, there are no obvious air voids exist inside the particles. Therefore, the rice grains are homogeneous and hard to break under confinement.

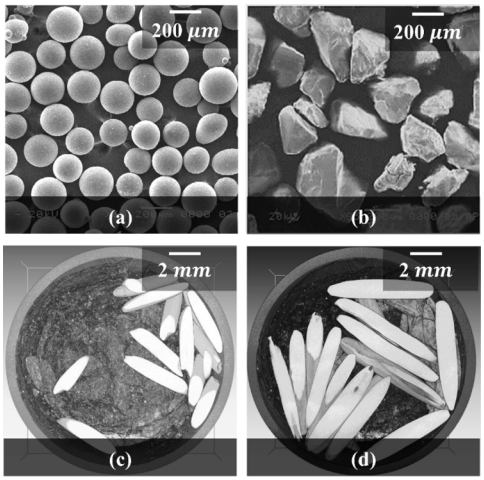

Figure 2. (a) SEM image of spherical glass beads, (b) SEM image of Toyoura sand, (c) micro-CT image of basmati rice, and (d) micro-CT image of wild rice.

3. Apparatus and testing program

3.1. Eight-prismatic membrane cell and specimen preparation

To directly measure the V_{phase} of S-waves in both principal and oblique directions, the eight-prismatic membrane cell was developed in this study. As shown in Fig. 3, there are five pairs of opposite faces of the membrane cell, among which three pairs of faces are perpendicular to principal directions *X*, *Y*, and *Z*, and another two pairs of faces are perpendicular to the direction 45° to the vertical axis. The distance between each pair of the opposite faces is 125 mm except in the vertical direction, where an extra 30 mm in height (thus, a total of 155 mm) was added to facilitate specimen preparation. The total flexible boundary of this testing apparatus can alleviate extra measured anisotropy induced by a mix of rigid and flexible boundary conditions and precisely measure the V_{phase} of S-waves (Liu et al., 2022).

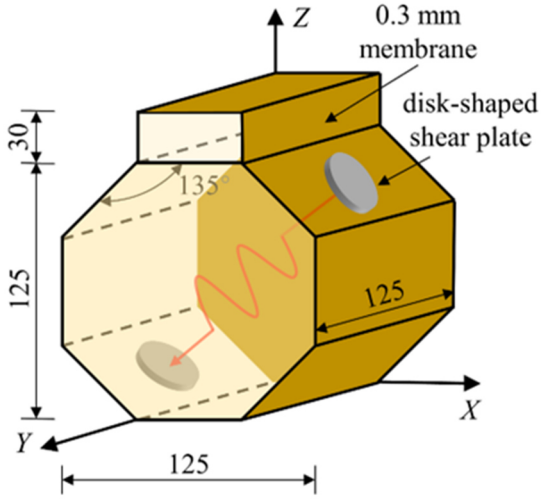

Figure 3. Schematic of the eight-prismatic membrane cell (unit: mm).

During the specimen preparation, the customized 0.3 mm-thick eight-prismatic latex membrane was stretched to the 3D-printed mold (Fig. 4) and the air between them was vacuumed out to ensure that the membrane was perfectly fitted to the inner mold wall. Then the tested material was air-pluviated into the membrane cell and was tamped by a wooden tool layer by layer for a total of 10 layers to achieve a dense packing. After the preparation, another piece of the membrane was pasted to the top to close the cell and the whole specimen was vacuumed to apply an isotropic confining stress of 50 kPa. The relative densities of the four specimens are all over 65% after confinement.

For the measurement of V_{phase} of S-waves, a circular opening with a diameter of 20 mm was cut at the center of each pair of opposite membrane faces before the specimen preparation, and a 2-mm-thick acrylic sheet was pasted behind the opening. During the S-wave propagation test, a pair of disk-shaped shear plates were pasted to the sheet by double-sided adhesive tape rather than directly to the membrane. This connection method

ensures a firm attachment and better S-wave signals that can be received during experiments. The use of double-sided adhesive tape can make it easier to remove the transducers from the specimen and adjust them to measure S-waves with other propagation or oscillation directions.

Figure 4. Customized eight-prismatic latex membranes of 3D printed mold.

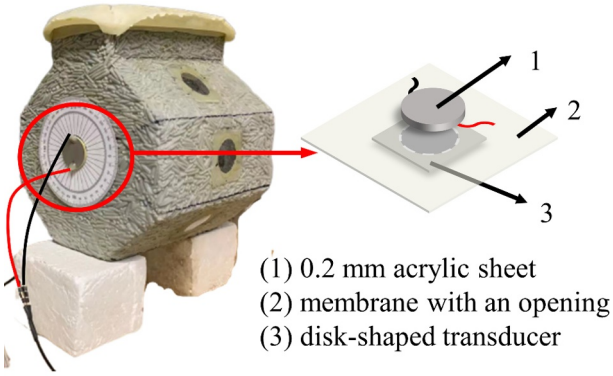

Figure 5. The eight-prismatic membrane cell and the attachment between the specimen and disk-shaped S-wave transducers.

3.2. S-wave propagation tests

As can be seen from Fig. 3, S-waves always travel perpendicularly to the two parallel disk-shaped shear plates. Therefore, V_s calculated from the distance between the opposite shear plates and the corresponding travel time is the V_{phase} regardless of the propagation direction. Referring to Fig. 6, ten types of S-waves can be measured in the eight-prismatic membrane cell. Specifically, the eight S-wave components propagating within the XZ plane can be separated into two groups based on the oscillation direction. The first group includes components S_{xy} , S_{45y} , S_{zy} , and S_{135y} that oscillate along the Y axis. The second group contains components S_{xz}, S_{45xz}, S_{zx}, and S_{135xz} that oscillate within the XZ plane. The categorization will facilitate the discussion of correlations between soil inner fabric and S-wave propagation and oscillation directions. Since S-wave can travel through two oblique paths at 45° to the Z axis, one traveling path is denoted as 135° for the distinguishment of S-wave notations.

A single period of sinusoidal pulse with a double amplitude voltage of 140 V was used to generate S-waves from the transmitter transducer. Following the method described in Dutta et al. (2019) to determine the optimum input frequency, f_{in} = 10 kHz was selected to measure S-waves in glass beads and Toyoura sand specimens, while f_{in} = 5 kHz was chosen for the two rice specimens since signals with high frequencies are difficult to propagate through large particles (Liu et al., 2022). In addition, the wavelength calculated from the above-mentioned f_{in} and the corresponding V_s is three times longer than the average particle length in the major axis for all the tested materials. This is to reduce S-wave scattering during propagation and to improve the received signal quality, as recommended by ASTM D 2845-00 (2000).

The peak-to-peak method was adopted in this research to determine the travel time of S-waves by calculating the time difference between the first major peaks of the input and output signals, as illustrated in Fig. 7.

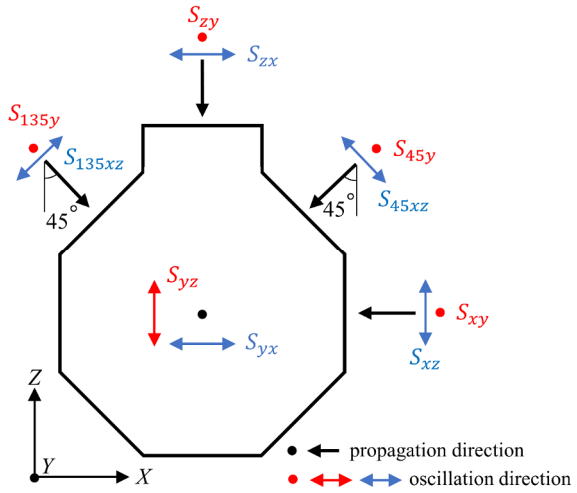

Figure 6. Schematic of the ten S-wave components measured from the eight-prismatic membrane cell.

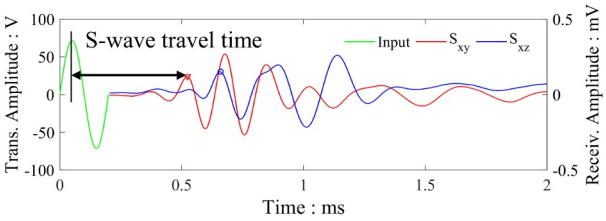

Figure 7. Typical S-wave signals obtained in this research and the peak-to-peak travel time determination method.

4. Experiment results and discussions

Although ten components of S-waves were measured in the eight-prismatic membrane cell, this article will mainly discuss the small-strain stiffness anisotropy of tested materials (indicated by the variation of V_s) based on the two groups of S-waves as categorized in section 3.2. Generally, the ratio of V_s in the horizontal plane to that in the vertical plane can be used to quantitively characterize the degree of stiffness anisotropy of the tested material (Fioravante, 2000; Liu et al., 2022).

4.1. Glass beads

Among the four tested materials, glass beads are the most rounded and are expected to display relatively isotropic behavior under isotropic confinement.

However, $V_{s,xy}/V_{s,zy}$ = 1.06, indicating a small degree of stiffness anisotropy. Correspondingly, the V_s surface plotted through S-waves oscillating along the Y axis is slightly elliptical as shown in Fig. 8. The measured stiffness anisotropy may be induced by the layering of materials during the specimen preparation process or the complex shape of the eight-prismatic specimen. The differences between the two pairs of symmetric components, $V_{s,xz}/V_{s,zx}$ = 1.05 and $V_{s,45xz}/V_{s,135zx}$ = 1.03, are relatively small, which confirms the assumption that granular soils are cross-anisotropic at small strains.

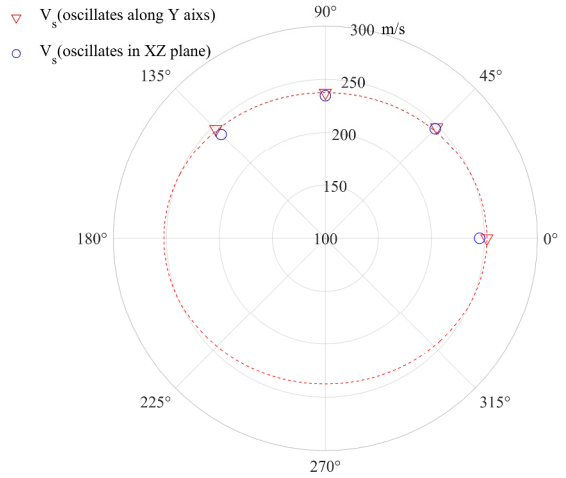

Figure 8. Polar plot of V_s in glass beads specimen.

4.2. Toyoura sand

Although Toyoura sand is more angular compared with the glass beads, the V_s surface plotted through S-waves oscillating along the Y axis is almost circular as demonstrated in Fig. 9. The $V_{s,xy}/V_{s,zy}$ = 1.02, showing very weak anisotropic responses. Liu et al. (2022) also reported a very small degree of stiffness anisotropy ($V_{s,xy}/V_{s,zy}$ = 1.03) in Toyoura sand enclosed in a cubical membrane cell and confined under 50 kPa. However, Wang and Mok (2008) recorded obvious anisotropic S-waves in Toyoura sand tested by a rigid boundary cubical box under isotropic confinement, in which $V_{s,hh}/V_{s,vh}$ = 1.09. The reason why Toyoura sand shows relatively isotropic responses should be further checked.

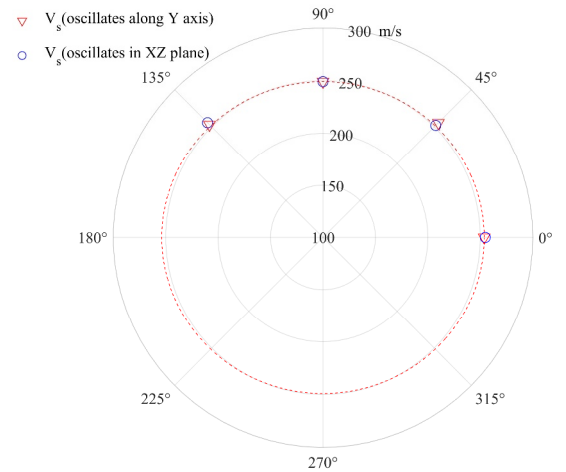

Figure 9. Polar plot of V_s in Toyoura sand specimen.

4.3. Basmati rice

The V_s surface of basmati rice is quite elliptical since the elongated particles induced strong fabric anisotropy ($V_{s,xy}/V_{s,zy}$ = 1.29) during the specimen preparation (Fig. 10). As can be seen from Fig. 10, V_s of S-waves oscillating along the Y axis decreased accordingly when the propagation direction changed from horizontal to vertical, confirming that the majority of rice particles bedded in the horizontal XY plane. V_s of S-waves within the vertical XZ plane are almost the same regardless of the strong initial fabric anisotropy, which is following the cross-anisotropic assumption of soils.

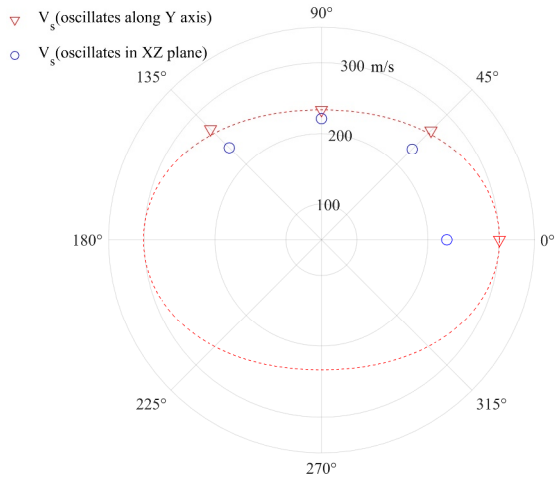

Figure 10. Polar plot of V_s in basmati rice specimen.

4.4. Wild rice

The wild rice displayed the strongest fabric anisotropy ($V_{s,xy}/V_{s,zy}$ = 1.57) among the four tested materials because of its more elongated particle shape, resulting in thinner elliptical V_s surface compared with that of basmati rice as shown in Fig. 11.

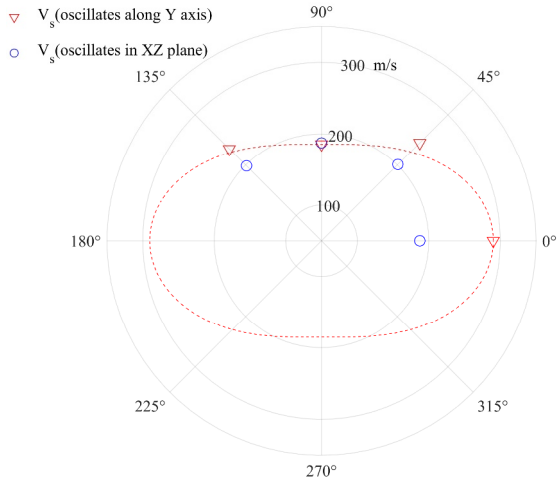

Figure 11. Polar plot of V_s in wild rice specimen.

4.5. Discussions

4.5.1. Fitting equation of V_s surface

Zeng and Ni (1999) derived the following equation based on the elastic constitute model proposed by Hardin and Blandford (1989) to predict V_s along any propagation path with an angle α to the horizontal plane:

$$V_{s,\alpha}=V_{s,h}V_{s,v}/\sqrt{V_{s,h}sin^2\alpha+V_{s,v}cos^2\alpha} \quad (3)$$

where $V_{s,h}$ and $V_{s,v}$ are S-wave velocities in the horizontal and vertical paths, respectively.

This equation was used to plot the V_s surfaces of the four granular materials in this study. As shown in Fig. 8 to Fig. 11, all the V_s measured from the two oblique directions in each material are slightly beyond the surface, which indicates that the measured stiffness anisotropy by the eight-prismatic membrane cell is a little smaller than the theoretical predictions (less elliptical V_s surfaces if the data points are best fitted by elliptic curves). However, the equation is still applicable to evaluate the small-strain stiffness anisotropy of a given soil.

4.5.2. Effects of particle shape on S-wave anisotropy

According to Fig. 12, the ratio of $V_{s,hh}/V_{s,vh}$ increases with the decrease of particle aspect ratio. In other words, more elongated particle shape can induce larger initial fabric anisotropy under isotropic confinement. This trend is consistent with the experimental observation reported by Liu et al. (2022) and the simulation work conducted by Otsubo et al. (2020).

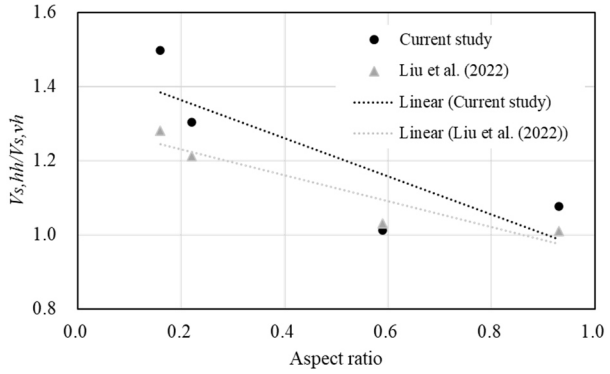

Figure 12. Relationship between S-wave anisotropy and particle shape.

4.5.3. Limitations of Experimental setup and measurement uncertainties

The eight-prismatic membrane cell contains another two pairs of opposite inclined faces compared with the traditional cubical membrane cell. The inclined faces may influence the initial soil fabric because granular particles near the boundaries tend to orient along the inclined faces. Therefore, the effects of complex specimen shape on the small-strain stiffness anisotropy of soils should be further examined.

The measurement uncertainties of V_s are mainly from two aspects. First, the shrinkage of the specimen edges after mold disassembly and the membrane penetration made it difficult to precisely measure the S-wave travel distance and specimen volumes. Second, the determination of S-wave travel time can also introduce some errors because the first peaks of received signals were selected manually.

5. Conclusions

This study described a novel eight-prismatic membrane cell equipped with disk-shaped shear plates which can be used to measure V_s and evaluate small-strain stiffness anisotropy of soils. Glass beads, Toyoura sand, basmati rice and wild rice with different particle shapes were tested by the apparatus to verify its capability.

Experimental results confirm that the newly-developed apparatus is capable of precisely measuring the V_{phase} of S-waves in both principal and oblique directions. The polar plot of V_{phase} of S-waves having the same oscillation direction but various propagation directions can properly reflect the sitffness anisotropy of tested materials, while the V_{phase} in the vertical XZ plane can be used to check the conformity of soils to the cross-anisotropic assumption within small-strain range. Since both S-wave propagation direction and oscillation direction are sensitive to the soil fabric, it is recommended to S-waves with same oscillation direction to plot the anisotropic V_s surface.

Acknowledgements

The authors are grateful for the financial support provided by SPRING GX project of the University of Tokyo. The project presented in this article is supported by JSPS KAKENHI Grant Number 22K14322.

References

ASTM D2845-00. Standard Test Method for Laboratory Determination of Pulse Velocities and Ultrasonic Elastic Constants of Rock, ASTM International, West Conshohocken, PA, 2000

Bellotti, R., Jamiolkowski, M., Lo Presti, D. C. F. and O'Neill, D. A. "Anisotropy of small strain stiffness in Ticino sand," Geotechnique, 46(1), pp.115-131, 1996. https://doi.org/10.1680/geot.1996.46.1.115

Chamorro-Zurita, C., & Ovando-Shelley, E. Anisotropy of lacustrine soils in a large oedometer equipped with bender elements. Soils and Foundations, 60(2), pp.372-383, 2020. https://doi.org/10.1016/j.sandf.2020.02.009

Dutta, T. T., Otsubo, M., Kuwano, R., & O'Sullivan, C. Stress wave velocity in soils: Apparent grain-size effect and optimum input frequencies. Géotechnique Letters, 9(4), pp.340-347, 2019. https://doi.org/10.1680/jgele.18.00219

Fioravante, Vincenzo. "Anisotropy of small strain stiffness of Ticino and Kenya sands from seismic wave propagation measured in triaxial testing." Soils and foundations, 40(4), pp. 129-142, 2000. https://doi.org/10.3208/sandf.40.4_129

Hardin, B. O., & Blandford, G. E. Elasticity of particulate materials. Journal of Geotechnical Engineering, 115(6), pp.788-805, 1989. https://doi.org/10.1061/(ASCE)0733-9410(1989)115:6(788)

Lee, Jong-Sub, and J. Carlos Santamarina. "Bender elements: performance and signal interpretation." Journal of Geotechnical and geoenvironmental engineering 131(9), pp.1063-1

070, 2005. https://doi.org/10.1061/(ASCE)1090-0241(2005)131:9(1063)

Liu, J., Otsubo, M., Kawaguchi, Y., & Kuwano, R. Anisotropy in small-strain shear modulus of granular materials: Effects of particle properties and experimental conditions. Soils and Foundations, 62(1), 101105, 2022. https://doi.org/10.1016/j.sandf.2021.101105

Nemat-Nasser, S., & Takahashi, K. Liquefaction and fabric of sand. Journal of Geotechnical engineering, 110(9), pp.1291-1306, 1984. https://doi.org/10.1061/(ASCE)0733-9410(1984)110:9(1291)

Nishimura, S., & Abdiel, M. D. Cataloguing stiffness anisotropy of natural sedimentary soils–From clays to intermediate soils. Japanese Geotechnical Society Special Publication, 5(2), pp.101-106, 2017. https://doi.org/10.3208/jgssp.v05.021

Otsubo, M., Liu, J., Kawaguchi, Y., Dutta, T. T., & Kuwano, R. Anisotropy of elastic wave velocity influenced by particle shape and fabric anisotropy under K0 condition. Computers and Geotechnics, 128, 103775, 2020. https://doi.org/10.1016/j.compgeo.2020.103775

Sadek, T., Lings, M., Dihoru, L., & Wood, D. M. Wave transmission in Hostun sand: multiaxial experiments. Rivista Italiana Geotecnica, 41(2), pp.69-84, 2007.

Yang, J., & Gu, X. Q. Shear stiffness of granular material at small strains: does it depend on grain size?. Géotechnique, 63(2), pp.165-179, 2013. https://doi.org/10.1680/geot.11.P.083

Zeng, X., & Ni, B. Stress-induced anisotropic G max of sands and its measurement. Journal of geotechnical and geoenvironmental engineering, 125(9), pp.741-749, 1999. https://doi.org/10.1061/(ASCE)1090-0241(1999)125:9(741)